Conference on Modelling Fluid Flow (CMFF'25)
The 19th International Conference on Fluid Flow Technologies
Budapest, Hungary, August 26 - August 29, 2025

FLUID MECHANICS OF CEREBRAL THROMBI

László FUCHS[1], Lisa PRAHL-WITTBERG[2]

[1] Corresponding Author. Department of Mechanics, KTH, Royal Institute of Technology, Stockholm, Sweden. Tel.: +46 705728466, E-mail: fuchs@kth.se
[2] Department of Mechanics, KTH, Royal Institute of Technology, Stockholm, Sweden. Tel.: +46 736756464, E-mail: prahl@kth.se

ABSTRACT

Blood flow in a typical human aorta is considered by numerical simulations. Thrombi fragments (emboli) may reach the arteries leading blood to the brain. The flow in the aorta depends on the geometrical details and the temporal flow rate due to the cardiac output and the outflow from the branching arteries. Aortic flow is unsteady, swirling and may have a retrograde component during parts of the cardiac cycle. Retrograde flow may transport emboli into the branching arteries leading to the brain. Such a situation may occur also for particles, released late in diastole even when released in the descending aorta. The risk of stroke due to retrograde transport has also been observed clinically. Here, we simulate numerically the risk for emboli as a function of different heartbeat types. Particles with different properties were inserted, at different locations and at different time instants during the cardiac cycle. The motion of the particles and the forces acting on them may be used to assess risk for cerebral stroke. The temporal characteristic of the cardiac flow is an important stroke risk factor. It is shown that some clinical reports may underestimate the risk of stroke in thoracic aorta with small plaques (< 4 *mm*).

Keywords: Cerebral embolus. CFD, LPT, Thoracic aorta, retrograde particle transport.

NOMENCLATURE

inlet	[-]	The inlet plane
F_D,F_L	[*N*]	Forces acting on a particle
$F_{Saffman}$	[*N*]	Saffman lift force
F_{mass}	[*N*]	Added mass force
C_D	[-]	Drag coefficient
BC	[-]	Brachiocephalic artery
LC	[-]	Left Carotid artery
LS	[-]	Left Subclavian artery
Exit	[-]	Portion of particles leaving
Remain	[-]	Portion of particle within the aorta
IP1-IP4	[-]	Injection Points (Figure 3).
Re_p	[-]	Particle Reynolds number

1. INTRODUCTION

Stroke due to embolism may occur when a blood clot reaches a major artery supplying blood to the brain. The aortic arch has three major branches: the Brachiocephalic (BC) left Carotid (LC) and left subclavian (LS) arteries. All three arteries are major blood suppliers to the brain. Thus, blood clots from the heart, the ascending aorta, the aortic arch, or the proximal part of the descending aorta are all potential sources for ischemic stroke. Yet, it is not obvious whether a blood clot may enter BC, LC and LS at all. Atheroma in the proximal parts of the thoracic aorta, and in the aortic arch has often been observed in ischemic stroke patients when the atheroma diameter is larger than 4 *mm* [1].

Further evidence for the relation between aortic atheroma and the risk for ischemic stroke has been accumulated over the past decades [3-10]. The observations presented in these references suggested that retrograde diastolic blood flow in the proximal descending aorta having larger plaques (> 4 *mm*) could be associated with brain embolism due to retrograde aortic flow. Such retrograde flows in the aortic arch and proximal descending aorta were observed and characterized several decades ago using ultrasound technique [10-11].

Geometrical details of the aortic arch branching play an important role in ischemic stroke. In general, it has been observed that the percentage of left-sided infarcts are more common. Elsaid et al [12] classified the branches of the aortic arch into three types. The main finding was that cardio emboli caused by atrial fibrillation tends to have left anterior cerebrovascular predilection. Similarly, Xu et al [13] studied the relationship between the different aortic arch types (i.e., geometrical shapes) and the location of large vessel occlusion (LVO) in cardioembolic stroke. It was found that the anatomical shape by itself is inadequate to determine the risk for ischemic stroke. In addition to the shape of the aorta, its mechanical properties (i.e. aortic wall stiffness) and the temporal behavior of the cardiac output affect the extent of flow reversal [14].

The clots found in arteries vary considerably in shape and composition depending on the formation and degradation process that takes place naturally. In-vitro measurements of clots by Nahirnyak et al [15] reported the averaged clot density to be 1.08 10^3 kg/m^3 with an overall uncertainty in the density measurements of about 2%. Thrombi containing large volumes of fibrin have higher density, up to 1300 kg/m^3. The computation study by Choi et al [16], using the data of Nahirnyak et al [15] assumed thrombus size and density of 2-6 *mm* and 1080 kg/m^3, respectively. Pennati et al [17] and Neidlin et al [18] investigated numerically thrombectomy and endovascular mechanical recanalization, using thrombus density of 1300 kg/m^3.

The mechanism of clot transport depends both on the geometrical details of the thoracis aorta and the associated blood flow in it. The spatial and temporal details of the flow reveal the extent and variations of blood flow reversal. Fuchs et al [19-20] studied the volumetric extent of retrograde flow in the thoracic aorta for different cardiac flow rate profiles, concluding that details of the temporal behavior of cardiac flow profile impact on retrograde flow volume more than heart rate (HR) and cardiac output (CO). It was found that ratio of retrograde flow volume relative to the aortic volume depends on time and the character of the temporal variations in the cardiac cycle. Peak retrograde volume was reached at the local minimum of the volumetric flow. Peaks of wall shear-stress were observed at time instances when the time-derivative of the retrograde volume had (instantaneously) large temporal derivative. Rapid deceleration and elevated HR/CO were found to promote retrograde flow when expressed in terms of backflow volume relative to the total aortic volume. Although this measure may not directly reflect the potential of upstream thrombus transport, it raises the question of, and motivates investigating, the influence of retrograde flow dynamics on thrombus transport. The purpose of the current study was to assess the risks for ischemic embolus due to CO-pathology conditions, clot size and density, clot detachment location and instant during the cardiac cycle. The study is based on numerical flow simulations along with corresponding study of particle transport, depending on particle size, density, motion unsteadiness and local shear of the fluid.

The main purpose of this paper was to expose the basic fluid mechanical driving mechanism responsible for transport processes in the thoracic aorta and that may lead to cerebral stroke. These aspects were assessed by tracking solid spherical particles released at some specific locations and at certain times of the cardiac cycles. The cardiac flow rate was kept constant (1 Hz), but the temporal flow-rate distribution was changed such that the effects of deceleration and flow recovery on particle transport could be assessed. The modified cardiac output profiles are used to emulate heart arrhythmia.

2. Methods

The numerical simulations were carried out using a typical geometry of a generic human thoracic aorta (Swedish ethical approval Dnr 2017/258-31). The aortic walls were assumed to be rigid. The thoracic aorta has three major arteries, branching from the aortic arch (Figs 2-3.). These arteries lead blood to the upper parts of the body and to the brain. The flow distribution among the different branches may vary, depending on individual and instantaneous conditions. In the following simulations, the blood flow rate over the cardiac cycle was kept to 5 l/min. The temporal distribution into the inlet corresponded to the flow rate suggested by Benim et al [21]. The flow distribution among the four outlets was set to 15%, 7.5%, 7.5% and 70%, for BC, LC, LS and the exit from the proximal, thoracic part into its abdominal part of the aorta, respectively.

The blood was assumed to be an incompressible, homogenous non-Newtonian liquid with constant density (1102 kg/m^3). The non-Newtonian effect was accounted for through the Quemada model [22], which is based on the local red blood cell concentration and the shear-rate. In the following computations, only the strength of local shear-rate affects the local blood viscosity.

The computational geometry was discretized on a sequence of grids. After evaluation of the accuracy on different grids (Fuchs et al [19-20]), a grid with about 6 million computation cells was used. Given the assumptions made on the blood and the geometrical set-up, the incompressible Navier-Stokes equations were discretized on the final mesh. The equations were integrated in time over several cardiac cycles to eliminate initial condition effects.

The computed results were used to assess particle transport from different locations and different particle properties. Particle transport was simulated in post-processing mode, repeating the final cardiac cycle several times (between 5 to 50 cardiac cycles), depending on the injection mode and location. Commonly, one assumes that the main force acting on particles is the drag force. However, after estimating the effects of flow unsteadiness and the shear-rates found in the simulated cases, we used the contribution of different forces, when accounting for the motion of particles in the aorta. The particle equations are given in the section below.

2.1 Particle tracking and forces

Newton's second law expresses the balance of forces acting on a solid spherical particle and its acceleration:

$$F_p = m_p \frac{du_p}{dt} = F_D + F_{press} + F_{mass} + F_L \quad (1)$$

where F_p, is the force acting on the particle m_p, and u_p are the mass and velocity of the particle; F_D,

F_{press}, F_{mass} and F_L are the considered forces acting on the particle due to drag, pressure gradient, added (virtual) mass and lift, respectively. For a wide range of Reynolds numbers, the drag force, F_D, can be expressed as:

$$F_D = \frac{1}{2} C_D \frac{\pi D_p^2}{4} (u_p - u)|u_p - u| \qquad (2)$$

where u and u_p are the local fluid and particle velocities, respectively. The drag is related to the relative velocity of the particle (u-u_p). The particle Reynolds number, Re_p, is defined as $Re=D_p|u-u_p|/\nu$, with $\nu = m/\rho_f$ being the kinematic viscosity, ρ_p and ρ_f are the density of the particle and the carrier fluid, respectively. As the particle Reynolds number, Re_p, is within the intermediate range (up to the order of 50-100) for the cases considered here, the drag coefficient, C_D was given by:

$$C_D = \begin{cases} \frac{24}{Re} & (Stokes\ flow:\ Re_p < 1) \\ \frac{24}{Re}(1 + 0.15Re^{0.687}) & 1 \le Re_p \le 10^3 \end{cases} \qquad (3)$$

The F_{press} term is related to the pressure gradient in the fluid phase and the volume of the (spherical) particle.

$$F_{press} = \frac{1}{6} \pi D_p^3 \nabla P \qquad (4)$$

The added mass force is due to the acceleration of the fluid, and for Stokes flow it equals to half of the particle mass times its acceleration:

$$F_{mass} = \frac{1}{12} \pi D_p^3 \rho_f \frac{du_p}{dt} \qquad (5)$$

The lift force is based on Saffman's expression and hence it is denoted in the following by $F_{saffman}$ (cf [23]).

$$F_{saffman} = K \rho_f D_p^2 \frac{-\sqrt{\nu}}{\sqrt{|\nabla \times u|}} ((\nabla \times u) \times (-u_p)) \qquad (6)$$

This form of the lift force is valid for small particle Reynolds numbers (Re_p) based on the local shear.

When hitting the aortic wall the particles were assumed to be reflected without losses.

3. COMPUTED CASES

In the following we consider the effects of the dynamics of blood flow in a model of human thoracic aorta, and its effect on the transport of spherical particles. All cases are for a cardiac output of 5 l/min at a rate of 60 beat per minute (1 Hz). The aortic shape was fixed for the computed cases. The following four different cases considered herein, differing from each other in terms of the temporal flow rate over the cardiac cycle: Case A stands for a common, periodic cardiac cycle. Case B is like case A, but with an abrupt termination of the late part of the systole, corresponding to a stop in blood pumping in the late part of systole. Case C is similar also to Case A bout with a 20% shorter diastole whereas Case D has a 20% longer diastole. Case B implies a fast deceleration of the flow, leading to strong adverse pressure in the aorta. The latter two cases are common to patients with cardiac arrythmia and may occur randomly or (less common) periodically. The four temporal volume flow rate vs time are depicted in Fig 1. The blood pumped into the thoracic aorta leaves the vessel through four exits, as described above.

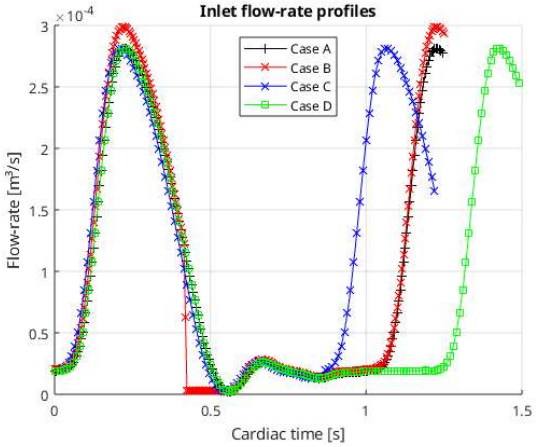

Figure 1. The volumetric flow rate into the aorta. Case A (black marking), "base" case with 60 beats/min and 5 l/min. The length of systole is roughly the same as the length of diastole. Case B (red markings) is like Case A, but with an abrupt termination of systole, leading to the formation of a sudden pressure increase. Case C (blue marking) is the same as Case A but with a 20% shorter diastole and Case D (green marking) has 20% longer diastole time.

The thoracic aorta has a significant curvature in the section termed as the aortic "arch" and a further weaker tortuosity in direction out of the plane of the arch. The curvature of the aorta implies formation of secondary flow. Further curvature out of the plane of arch leads to the formation of vortices of different scales. Time-dependency of the flow adds to the geometrical effects in terms of formation of additional vorticity.

Fig 2. depicts the instantaneous rotation (curvature) and angular velocity of particles released from a spherical region in the distal part of the aortic arch. Note the strong variation of these parameters along the particle paths. This observation, along with the clinical observation as discussed in the introduction, motivated the simulations to assess the interactions between the cardiac flow and particles with different sizes and densities.

The particles were released at four locations along the aorta (IP1 to IP4), as depicted in Fig 3. Particles injected into the aortic inlet were released continuously at the inlet plane. The number of particles leaving the four outlets increased until an asymptotic, final level was reached. These

simulations are useful to assess the accumulated impact of forces that the fluid exerts on the particles. A second mode, in which a given bolus of particles was released at certain instant of time within the cardiac cycle, was used to assess the risk for embolism from releasing particles at the different location at given time instance.

The injected particles were tracked by integrating Eqs (1) to (6) in a post-processing mode. Particles could leave the computational domain through the four exits mentioned above (BC, LCC, LSC and Exit). The injected particles were followed over five cardiac cycles with integration time-step of 1% of the cardiac cycle-time. The total integration time was long enough not to affect the total number of particles existing, the thoracic aorta segment under consideration. The accumulated number of particles leaving each exit plane relative to the number of injected particles was defined as the "Escape Rate" (ER). This criterion was used to reflect the risk for cerebral embolism.

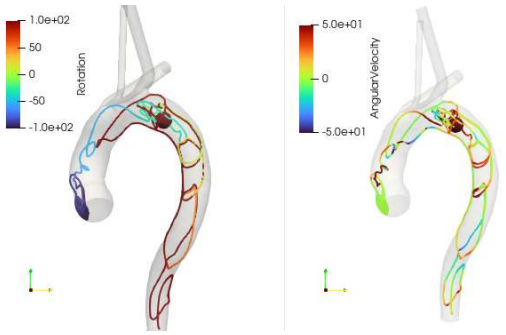

Figure 2. The instantaneous values of rotation and angular velocity on the particle paths. The particles were released from the spherical object downstream of the bifurcating arteries from the aortic arch.

Figure 3. Particles were released at the marked locations (denoted by IP1 to IP4, respectively): The aortic inlet was used to inject particles continuously throughout the simulation at the inlet plane. The evolution of the number of particles leaving each outlet followed in time, over ten to fifty cardiac cycles. In all other cases particles were injected at the marked location only once at a given instant of time in the cardiac cycle (after long enough simulations to attain a periodic flow field). These particles were followed over fine cycles only to assess the portion of particle leaving the different arteries branching from the aortic arch.

In the following we consider injection of particles particle injection into the aortic inlet (IP1), the arch (IP3) and the proximal descending aorta (IP4). The injected particles had the diameter of 2*mm* or 5*mm* and density of 1080 kg/l or 1200 kg/l, respectively. In each simulation, initial computation was carried out such that the effects of initial conditions were eliminated.

Table 1. shows the number of particles leaving the four outlets, relative to the total number of injected particles (ER). Inlet injection was continuous (i.e. throughout the cardiac cycle), and the number of particles was accumulated over time until a balance between injection rate and ER is in balance. The Escape Rate in the table was computed by following particles injected at the entrance to the aorta and during 10 cardiac cycles. As noted, the particle size is more important than the particle density. We also note that the large number of the larger (5*mm*) particles as well as the large portion of remaining smaller particle left through the Brachiocephalic (BC) artery.

The impact of the cardiac cycle on particle transport depends strongly on particle density and size. Irregular cardiac cycles (e.g. Cases C and D) lead to stronger transport of the 2*mm* particles through the aorta. The effect was much smaller for the 5*mm* particles. The risk for transport into the most distal (the left subclavian, LS) artery is almost twice as large for the irregular cardiac cases as compared to the periodic (Case A) cardiac rhythm.

When assessing the risk for embolus transport into the arteries branching from the aortic arch, a single bolus of particles was injected for each particle type at certain instant of time. Table 2 shows the portion of particles leaving the aorta accumulated over five cardiac cycles. The table corresponds to an injection point at the aortic arch (IP3) and at 50% of the cardiac cycle (i.e. approximately the end of systole, IT=0.5). As noted, and as expected most particles leave the aorta in the streamwise direction. The risk for stroke is non-negligible for the larger (5 *mm*) particles. A premature heartbeat (Case C) leads to elevated stroke risk also for the 2 *mm* particles. Particles released at other locations further downstream show similar behavior as shown in Table 2. Particles released further downstream in the ascending part of the aorta do not reach upstream, provided that the release instance takes place before mid-diastole. Fig. 4 depicts particle locations after five cardiac cycles, when the particles are released at the most distal location (IP4, shown in Fig. 3). Three different particle injection instances are shown: Release time at IT=0.25, 0.5 and 0.75 s (equals to

percentages of the time in the cardiac cycle). The particles are colored by the (Frobenius) norm of the stress tensor acting on the particle instantaneously.

Early injection instants (i.e. during systole) lead to the advection of the particles downstream with low degree of retrograde flow that is inadequate to transport particles in the arteries of the aortic arch. Late injection times, such as the one shown in Fig. 4 with IT= 0.75 s, leads to considerable retrograde flow. As the particles are injected during diastole, they are sucked upstream directly. During the next systolic phase (1< T <1.5 s) the particles are transported into all three branching arteries. Repeated simulations show that the highest probability for embolus is through the left subclavian (LS) artery. Indeed, the simulations do confirm clinical observation of higher stroke incident rate through the LC artery [12].

The stress acting on the particles may be large initially, depending on the relative velocity between the blood flow and the stationary thrombus. This stress determines also possible instant of fragmentation of the thrombus, and which is affected by the mechanical property of the thrombus. The norm of the stress acting on the particles increases over time and exceeds in all cases 1 N/m^2. The impact of stress on the particles was not considered here and can be seen as be a limiting factor in the simulations herein.

5. DISCUSSION

The results may be divided primarily into the fluid-mechanical aspect and secondly on potential clinical impact. The results demonstrate that the transport of spherical, rigid particles depends not only the commonly assumed drag, but also the rate of flow deceleration during the cardiac cycle. The deceleration affects enters both into the added mass and the Saffman terms (Eqs (5) and (6)). The results clearly demonstrate the role of retrograde, near-wall flow to transport particles upstream in the thoracic aorta. The results also help in explaining the elevated embolus risk heart arrythmia with prolonged diastole followed by a normal systole. The clinical impact of this work implies that the physical properties and the embolus (i.e. density and diameter) along with the detachment location and instant during the cardiac cycle strongly affect the risk for stroke. The multiple factors leading to stroke make it practically difficult to use patient-specific data to predict the risk for stroke.

The limitations of the study are due to the assumption made on the one-way coupling between the particles and the fluid. Further assumptions are made with respect to particle properties, solid aortic walls, particle-wall interaction and the limited variations in the imposed boundary conditions.

6. CONCLUSIONS

Detached thrombus fragments from the heart or the thoracis aorta was observed clinically as a potential risk for ischemic stroke (embolus). The simulations herein focus on the impact of particle size and diameter, release location and release instant of time in the cardiac cycle and not least irregularities in the cardiac cycle itself. The results indicate that the risk för stroke depends on all these parameters. Classification of stroke risk only by the aortic geometry as attempted clinically is inadequate, as the risk depends strongly also on the flow dynamics. The risk for stroke is very low for embolus released during systole and early diastole. Release in diastole implies risk for stroke with all four particle types. The results show that also smaller particles may lead to elevated stroke risk. This is in contrasts with clinical finings that the risk for stroke applies only for larger aortic atheroma with diameters larger than 4 *mm*.

ACKNOWLEDGEMENTS

Former Ph.D. students (Niclas Berg and Alexander Fuchs) assisted in the earlier stages of the project. Their contribution is highly acknowledged. The funding from the Swedish Heart Lung Foundation (Dnr 20220492) is highly acknowledged.

REFERENCES

[1] Viedma-Guiard, E, et al. Aortic Sources of Embolism. *Front Neurol.* doi: 10.3389/fneur.2020.606663, 2021, Vol. 15, 11:606663.

[2] Kronzon, I and Tunick, P. Aortic Atherosclerotic Disease and Stroke. *Circulation.* doi:10.1161/CIRCULATIONAHA.105.593418, 2006, Vol. 114, 1:63-75.

[3] Harloff, A, et al. Complex plaques in the proximal descending aorta: an underestimated embolic source of stroke. *Stroke* . doi: 10.1161/STROKEAHA.109.577775, 2010, Vol. 41, 6:1145-1150.

[4] Chhabra, L, et al. Retrograde embolism from the descending thoracic aorta causing stroke: an underappreciated clinical condition . *Indian Heart J.* . doi:10.1016/j.ihj.2013.04.024, 2013, Vol. 65, 3:319-322.

[5] Wehrum, T, et al. Aortic atheroma as a source of stroke –assessment of embolization risk using 3D CMR in stroke patients and controls. *J Cardiovascular Magnetic Resonance.* DOI:10.1186/s12968-017-0379-x, 2017, Vol. 19:67.

[6] Wehrum, T, et al. Measurement of cardiac valve and aortic blood flow velocities in stroke patients: a comparison of 4D flow MRI and echocardiography. *The international journal of cardiovascular imaging* . 2018, Vol. 34, 6:939-946.

[7] Wehrum, T, et al. Aortic Atherosclerosis Determines Increased Retrograde Blood Flow as a Potential Mechanism of Retrograde Embolic Stroke. *Cerebrovasc Dis.* doi: 10.1159/000455053, 2017, Vol. 43, 3-4:132-138.

[8] Wehrum, T, et al. Age dependence of pulmonary artery blood flow measured by 4D flow cardiovascular magnetic resonance: results of a population-based study. *J Cardiovasc Magn Reson* . doi:10.1186/s12968-016-0252-3, 2016, Vol. 18:31.

[9] Wehrum, T, et al. Quantification of Retrograde Blood Flow in the Descending Aorta Using Transesophageal Echocardiography in Comparison to 4D Flow MRI. *Cerebrovasc Dis* . doi: 10.1159/000381682, 2015, Vols. 39:287–292 .

[10] Kilner, P J, et al. Helical and Retrograde Secondary Flow Patterns in the Aortic Arch Studied by Three-Directional Magnetic Resonance Velocity Mapping. *Circulation.* 1993, Vol. 88, 5:2235–2247.

[11] Segadal, L and Matre, K. Blood Velocity Distribution in the Human Ascending Aorta. *Circulation.* 1987, Vol. 76, 1:90-100.

[12] Elsaid, N, et al. The Relation Between Aortic Arch Branching Types and the Laterality of Cardio-Embolic Stroke. *J Stroke Cerebrovasc Dis.* . doi:10.1016/j.jstrokecerebrovasdis.2020.104917., 2020, Vol. 29, 7:104917.

[13] Xu, L, et al. The relation between aortic arch branching types and the location of large vessel occlusion in cardioembolic stroke. *J Clin Neurosci.* doi: 10.1016/j.jocn.612 2021.05.013, 2021, Vols. 89:171-176.

[14] Hashimoto, J and Ito, S. Aortic Stiffness Determines Diastolic Blood Flow Reversal in the Descending Thoracic Aorta: Potential Implication for Retrograde Embolic Stroke in Hypertension . *Hypertension.* 2013, Vol. 62, 3:542–549.

[15] Nahirnyak, VM, Yoon, SW and Holland, ChK. Acousto-mechanical and thermal properties of clotted blood. *J. Acoust Soc Am* . doi: 10.1121/1.2201251, 2006, Vol. 119:3766.

[16] Choi, HW, Navia, JA and Kassab, GS. Thrombus deflector stent for stroke prevention: A simulation study. *J Biomech. 2015,.* doi: 10.1016/j.jbiomech.2015.05.006. PMID: 26049978., 2015, Vol. 48, 10:1789-95.

[17] Pennati, G, et al. Numerical simulation of thrombus aspiration in two realistic models of catheter tips. *Artif Organs.* doi: 10.1111/j.1525-1594.2009.00770.x. , 2010 , Vol. 34, 4:301-10.

[18] Neidlin, M, et al. A numerical framework to investigate hemodynamics during endovascular mechanical recanalization in acute stroke. *Int J Numer Method Biomed Eng.* doi: 10.1002/cnm.2748, 2016, Vol. 32, 4:e02748.

[19] Fuchs, A, et al. The Impact of Heart Rate and Cardiac Output on Retrograde Flow in the Human Thoracic Aorta. *ASME J of Medical Diagnostics.* https://doi.org/10.1115/1.4054459, 2022, Vol. 5, 3:031107.

[20] Fuchs, A, Berg, N and Prahl Wittberg, L. Pulsatile Aortic Blood Flow—A Critical Assessment of Boundary Conditions. *ASME J. Med. Diagn.* 2020, Vol. 4:011002, doi: 10.1115/1.4048978.

[21] Benim, AC, et al. Simulation of blood flow in human aorta with emphasis on outlet boundary conditions. *Applied Mathematical Modelling.* 2011, Vols. 35:3175–3188.

[22] Quemada, D. Rheology of concentrated disperse systems ii. a model for non-Newtonian shear viscosity in steady flows. *Rheologica Acta.* 1978, Vol. 17, 6:632-642 .

[23] Saffman, PG. The lift on a small sphere in a slow shear flow. *J Fluid Mechanics.* 1965, Vol. 22, 2:385-400.

Table 1: Continuous injection of particles at the *aorta inlet* (IP1), after 10 cardiac cycles. The relative escape rate (ER) from the outlet planes of the thoracis aorta, expressed in percents. The 2 *mm* and 5 *mm* particles are shown in the upper and lower tables, respectively. The portion of injected particles that are found in the thoracic aorta after 10 cardiac cycle is denoted as "Remain".

	Case A		Case B		Case C		Case D	
	1080	1200	1080	1200	1080	1200	1080	1200
Exit	37.4	36.6	37.0	36.3	44.1	43.3	43.3	42.6
BC	9.5	10.2	9.7	10.4	8.9	9.7	10.3	11.2
LC	6.3	6.7	5.7	6.4	5.0	5.4	5.8	6.0
LS	5.1	5.9	6.8	7.2	4.8	5.4	6.7	7.4
Remain	41.7	40.7	40.9	39.7	37.1	36.3	33.9	32.7

	Case A		Case B		Case C		Case D	
	1080	1200	1080	1200	1080	1200	1080	1200
Exit	25.9	24.4	23.9	22.8	44.1	26.1	31.7	28.7
BC	46.8	48.1	43.5	45.1	8.9	45.6	49.6	50.6
LC	6.5	7.1	4.4	4.7	5.0	8.0	7.3	8.4
LS	4.1	4.0	3.9	4.2	4.8	5.4	6.7	7.5
Remain	16.8	16.4	24.2	23.3	37.1	15.0	4.7	4.7

Table 2: Continuous injection of particles at the *aortic arch* (IP3), after five cardiac cycles. The relative escape rate (ER) from the outlet planes of the thoracis aorta, expressed in percents. The 2 *mm* and 5 *mm* particles are shown in the upper and lower tables, respectively. The portion of injected particles that are found in the thoracic aorta after 5 cardiac cycle is denoted as "Remain".

	Case A		Case B		Case C		Case D	
	1080	1200	1080	1200	1080	1200	1080	1200
Exit	99.1	98.9	99.5	99.4	94.2	94.7	99.8	99.9
BC	0.0	0.0	0.0	0.0	0.0	0.0	0.0	0.0
LC	0.0	0.0	0.0	0.0	0.0	0.0	0.0	0.0
LS	0.3	0.6	0.5	0.5	1.2	1.2	0.0	0.0
Remain	0.5	0.6	0.1	0.1	4.6	4.1	0.1	0.1

	Case A		Case B		Case C		Case D	
	1080	1200	1080	1200	1080	1200	1080	1200
Exit	92.0	91.7	95.3	95.0	93.8	93.7	95.0	93.8
BC	0.0	0.0	0.0	0.0	0.0	0.0	0.0	0.0
LC	0.0	0.0	0.0	0.0	0.0	0.0	0.0	0.0
LS	8.0	8.3	4.7	5.0	6.2	6.3	5.0	6.2
Remain	0.0	0.0	0.0	0.0	0.0	0.0	0.0	0.0

IT=0.25

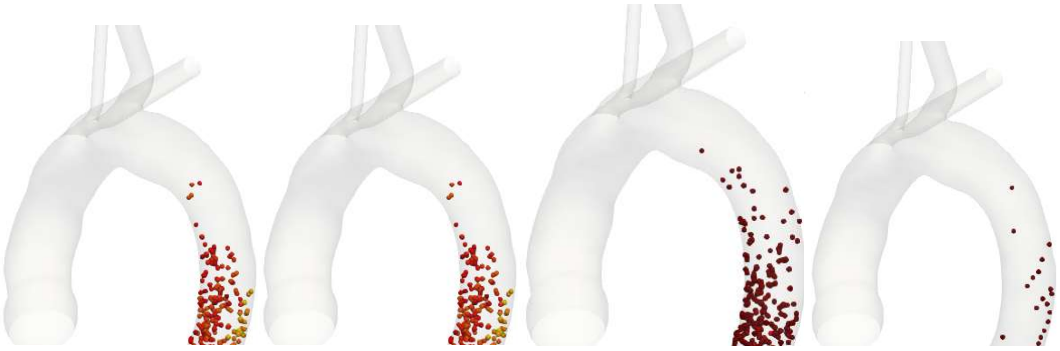

T=0.50 *T=0.75* *T=1.00* *T=1.50*

IT=0.50

T=0.50 *T=0.75* *T=1.00* *T=1.50*

IT=0.75

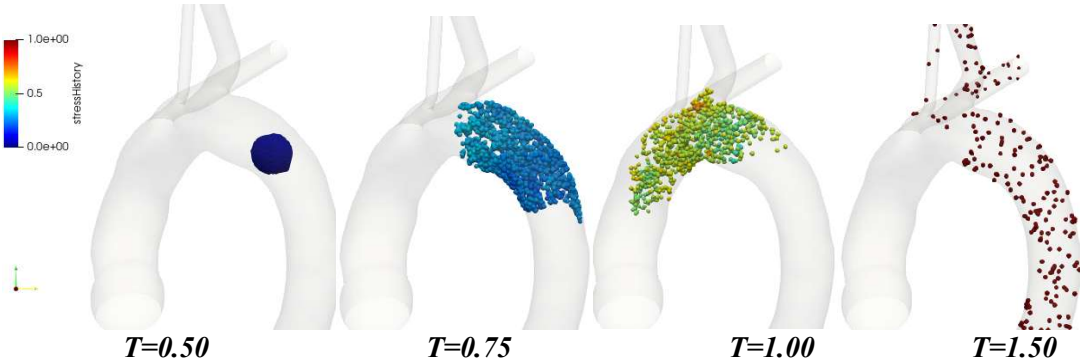

T=0.50 *T=0.75* *T=1.00* *T=1.50*

Figure 4. Injection of a single bolus of particles (Case A) at IP4, marked in left frame in the lowest row. There injection instants in the cardiac cycles are considered in the frames above: IT=0.25, 0.5 and 0.75 of the cardiac cycle, depicted in the three rows, respectively. The instantaneous particle positions, at different cardiac times are shown for each of the cardiac cycle instances is in the horizontal frames. T=0.75, 1, 1.25 and 1.5 stand for cardiac instant corresponding to about mid-diastole, end-diastole, peak- and end systole, respectively. Time T> 1, corresponds to the 2nd cardiac cycle. The injected particles were of density of 1080 kg/l and diameter of 5 *mm*. The norm of stress acting on the particles is used to color the particles (the colormap is shown in the low-left frame). Note (low-right frame) that particles that are injected in diastole are transported upstream into all three arteries that branch out from the aortic arch. Particles injected during systole do not end-up in the branching arteries.